SUPPLEMENTARY DATA

Effect of Repeated Glucagon Doses on Hepatic Glycogen in Type 1 Diabetes: Implications for a Bi-Hormonal Closed-loop System

Jessica R. Castle, MD[1]; Joseph El Youssef, MBBS[1]; Parkash A. Bakhtiani, MD[1]; Yu Cai, MD[2]; Jade M. Stobbe[2]; Deborah Branigan[1]; Katrina Ramsey, MPH[3]; Peter Jacobs, PhD[4]; Ravi Reddy, MSEE[4]; Mark Woods, PhD[2,5]; W. Kenneth Ward, MD[1]

[1]Department of Medicine, Division of Endocrinology, Harold Schnitzer Diabetes Health Center Oregon Health & Science University, Portland, OR
[2]Advanced Imaging Research Center, Oregon Health & Science University, Portland, OR
[3]Oregon Clinical and Translational Research Institute Biostatistics & Design Program, Oregon Health & Science University, Portland, OR
[4]Portland State University, Portland, OR
[5]Department of Biomedical Engineering, Oregon Health & Science University, Portland, OR

Model of Glucose and Insulin Kinetics

We used an established compartmental glucoregulatory model in the data analysis in this paper. This three compartment models utilizes sub models for the absorption of short acting insulin, insulin action on glucose kinetics and meals. The model provides a mathematical representation of the input-output relationship between the response to meals, intravenous dextrose delivery, intravenous insulin delivery, subcutaneous insulin doses given for each meal (inputs) and the venous glucose concentration (output). The model consists of a glucose kinetics model, insulin pharmacokinetic model and an insulin pharmacodynamic model. The model does not represent glucagon kinetics or dynamics.

The glucose kinetics model is implemented by a two compartment representation of the absorption, distribution and disposal of glucose. Gut absorption of meals is characterized by a two compartment system with identical transfer rate constants (estimated parameter) and carbohydrate bioavailability (estimated parameter).

The insulin kinetic model is comprised of insulin absorption, distribution and elimination subsystems (1). Subcutaneous administered insulin absorption is implemented using a two compartment model to estimate plasma insulin concentration. Intravenous insulin delivery is estimated to bypass the insulin kinetic model and enter the insulin action model directly. Insulin pharmacodynamics on glucose kinetics is described as three separate actions on glucose distribution/transport, disposal and endogenous glucose production, respectively. Insulin sensitivity parameters are defined for each of these individual actions. Insulin sensitivity for each action is defined as a ratio of activation rate constant divided by the deactivation rate constant. The glucoregulatory model consists of 19 model parameters and each parameter was estimated individually for each subject.

The model was developed using glucose tracer data and validated by Hovorka and colleagues (2).

SUPPLEMENTARY DATA

Fitting procedure:

Each data set from individual subjects was fit independently to the model. The model fit was performed for a period of ~18 hours for each subject, during this period 2 meals were consumed and one overnight period was included. Venous blood glucose values were available every 15 min, the insulin infusion rates/dextrose infusion rates were adjusted at each of these 15 min intervals based on the current glucose measurement.
The inputs to the model were the following time indexed vectors:

- meal carbohydrate amount (g)
- subcutaneous insulin infusion boluses (mU/kg/min)
- intravenous insulin delivery rate (mU/kg/min)
- intravenous dextrose delivery rate (mmol/kg/min)
- current glucose value (mg/dL)

The output from the model is

- predicted glucose value for the current set of inputs (mg/dL)

The upper and lower bounds for each of the parameter were defined as 175% and to 25% of the published values by Hovorka et al. (2).

The method of minimizing the absolute relative error was adopted for data fitting, which was implemented in Matlab (Mathworks, Natick) via the function *fmincon*. The glucoregulatory model described above was represented as a series of ordinary differential equations, which were solved numerically by Matlab. The cost function of optimization was defined as the mean absolute difference between the simulation output of the model and the measured clinical data at the sampled time points. The estimated optimal parameters for each subject were obtained when the cost function achieved its minimal value.

Based on the fitted parameters, glucose values for the entire study duration were estimated. Since the model does not include a glucagon component, the model estimations of the glucose values are expected to be lower than the measured glucose values following glucagon infusions. The model glucose estimations were subtracted from the measured unadjusted raw glucose values to create the adjusted glucose values. Both the unadjusted glucose values and the adjusted glucose values are time indexed values. The incremental area under the curve for the rise in glucose after each dose of glucagon was calculated for a period of 90 min after the dose using the trapezoidal method (3). The same methodology was adopted for both the adjusted glucose data and the unadjusted glucose data. This data is reported in a tabular form below. If repeated dosing of glucagon was causing depleted liver glycogen, then we would expect the area under the curve to decrease with subsequent doses of glucagon. Since glucagon was not included within the model, we do not expect the model estimate of glucose to be higher than the actual glucose. In certain instances, the model did predict a higher glucose value than the actual glucose which yielded a negative number in the adjusted data. We attribute these instances to inaccuracies in the model prediction based on an insufficient amount of data to train the model; only two meals are used to train the model and for the second meal we could not use the full response to the meal because glucagon was given shortly afterward. There are two ways to handle this model inaccuracy (1) by setting the adjusted glucose to zero or (2) by using a negative number as the adjusted glucose to calculate the AUC. We have presented results for both of these scenarios in the tables S1 and S2, respectively. Regardless of how this model inaccuracy is handled, there was no significant difference between AUC after the first dose of glucagon as compared the final dose of glucagon.

SUPPLEMENTARY DATA

Supplementary Table S1. Incremental AUC glucose data after each of 8 glucagon doses depicting unadjusted data, modeled glucose data, and adjusted data (unadjusted minus modeled). In this table, zeros are shown rather than showing negative adjusted glucose values.

Adjusted Data (Unadjusted – Modeled) ($mg \cdot min \cdot dL^{-1}$)								
	Dose 1	Dose 2	Dose 3	Dose 4	Dose 5	Dose 6	Dose 7	Dose 8
Subject 1	546	5402	3262	3193	773	4080	2327	3428
Subject 2	372	0	4215	333	3612	2342	5437	1076
Subject 3	1147	1982	3795	2354	4405	2109	4051	5770
Subject 4	300	5550	3780	7365	4058	3638	5370	2270
Subject 5	2114	1504	253	314	343	1205	328	1360
Subject 6	6360	3628	3449	6462	3379	1368	1692	1613
Subject 7	1417	4059	280	4369	3308	555	3090	3255
Subject 8	92	0	2834	5092	6004	5029	0	3835
Subject 9	4959	708	657	2566	3448	1060	1483	3221
Subject 10	419	0	1087	0	2105	2579	2208	3203
Subject 11	6574	1798	2894	4241	4286	6314	475	4171
Mean	**2209**	**2239**	**2410**	**3299**	**3247**	**2753**	**2406**	**3018**
SEM	**2512**	**2107**	**1526**	**2486**	**1635**	**1817**	**1908**	**1376**
Unadjusted Data ($mg \cdot min \cdot dL^{-1}$)								
	Dose 1	Dose 2	Dose 3	Dose 4	Dose 5	Dose 6	Dose 7	Dose 8
Subject 1	920	3690	2843	1215	135	4080	2460	3498
Subject 2	170	0	5115	45	3045	2340	5738	740
Subject 3	0	390	4185	2333	3945	2258	4125	6410
Subject 4	300	5550	3780	7365	4058	3638	5370	2270
Subject 5	965	1200	203	75	150	1328	623	1440
Subject 6	1725	3473	3353	4883	3090	570	2055	2225
Subject 7	1210	4733	0	4590	3210	555	3090	3255
Subject 8	1825	0	2040	3053	5250	3705	368	4475
Subject 9	2275	15	285	1215	3788	1433	1680	4065
Subject 10	60	0	1410	0	2490	3233	1575	2615
Subject 11	2840	4163	600	5663	195	6053	75	4100
Mean	**1117**	**2110**	**2165**	**2767**	**2669**	**2654**	**2469**	**3190**
SEM	**289**	**666**	**542**	**767**	**531**	**507**	**583**	**476**

Modeled Data ($mg \cdot min \cdot dL^{-1}$)								
	Dose 1	Dose 2	Dose 3	Dose 4	Dose 5	Dose 6	Dose 7	Dose 8
Subject 1	378	345	225	126	123	0	0	0
Subject 2	247	0	0	0	0	0	0	0
Subject 3	191	89	68	24	0	0	0	0
Subject 4	204	74	74	64	44	24	8	0
Subject 5	0	80	0	0	0	0	0	0
Subject 6	135	67	44	0	0	0	0	0
Subject 7	0	0	0	0	0	0	0	54

Subject 8	55	34	0	0	0	0	0	0
Subject 9	2	0	0	0	0	0	0	0
Subject 10	245	0	0	0	0	0	0	0
Subject 11	1026	499	49	37	0	0	0	0
Mean	226	108	42	23	15	2	1	5
SEM	293	163	68	40	38	7	2	16

Supplementary Table S2. Area under the curve for each dose of glucagon when including negative numbers in the adjusted AUC calculation. Glucose data after each of 8 glucagon doses depicting unadjusted data, modeled glucose data, and adjusted data (unadjusted minus modeled). Note that the unadjusted AUC was higher after the eighth glucagon dose, but after adjusting for lower insulin effect at that time point, there was no difference in AUC.

Adjusted Data (Unadjusted – Modeled) ($mg \cdot min \cdot dL^{-1}$)								
	Dose 1	Dose 2	Dose 3	Dose 4	Dose 5	Dose 6	Dose 7	Dose 8
Subject 1	-162	5402	3262	3118	363	4080	2327	3407
Subject 2	-979	-4528	4215	6	3612	2316	5437	974
Subject 3	1087	1975	3603	2290	4405	1911	4051	5770
Subject 4	-335	5550	3780	7365	4058	3638	5370	2245
Subject 5	2052	1099	-574	-441	-59	954	-132	1041
Subject 6	6360	2859	1961	6462	3379	1368	1388	1421
Subject 7	1259	4059	-76	4369	3308	285	3008	3255
Subject 8	-1754	-717	2834	5092	6004	5029	-638	3835
Subject 9	4959	451	-856	2566	3448	1041	1483	3221
Subject 10	241	-2848	499	-2896	2105	2579	2166	3146
Subject 11	6574	1798	2894	4241	4286	6314	-769	4171
Mean	**1755**	**1373**	**1958**	**2925**	**3174**	**2683**	**2154**	**2953**
SEM	**2926**	**3187**	**1872**	**3083**	**1771**	**1883**	**2193**	**1450**
Unadjusted Data ($mg \cdot min \cdot dL^{-1}$)								
	Dose 1	Dose 2	Dose 3	Dose 4	Dose 5	Dose 6	Dose 7	Dose 8
Subject 1	155	3690	2813	1005	-2258	4080	2460	3463
Subject 2	-2225	-5445	5115	-2273	3045	2303	5738	415
Subject 3	-1540	-1260	4163	2288	3945	2063	4125	6410
Subject 4	-335	5550	3780	7365	4058	3638	5370	2245
Subject 5	778	705	-968	-1005	-405	1028	248	1095
Subject 6	1635	2828	3353	4883	3090	38	1718	2225
Subject 7	875	4733	-1500	4590	3210	285	3008	3255
Subject 8	1825	-1598	1838	3053	5250	3705	293	4475
Subject 9	2255	-1245	-1988	1095	3788	1433	1680	4065
Subject 10	-460	-6488	1410	-5520	2490	3233	1500	2505
Subject 11	2775	4163	-653	5663	-1335	6053	-1935	4100
Mean	**522**	**512**	**1578**	**1922**	**2262**	**2532**	**2200**	**3114**
SEM	**1576**	**4089**	**2499**	**3794**	**2450**	**1814**	**2292**	**1674**

SUPPLEMENTARY DATA

Modeled Data ($mg \cdot min \cdot dL^{-1}$)								
	Dose 1	Dose 2	Dose 3	Dose 4	Dose 5	Dose 6	Dose 7	Dose 8
Subject 1	378	345	225	126	123	-3	-3	-7
Subject 2	247	-178	-152	-126	-104	-86	-75	-97
Subject 3	191	89	68	24	-15	-59	-123	-317
Subject 4	204	74	74	64	44	24	8	-17
Subject 5	-231	80	-132	-99	-89	-84	-83	-140
Subject 6	135	67	44	-104	-259	-320	-598	-833
Subject 7	-50	-296	-401	-568	-487	-375	-342	54
Subject 8	55	34	-9	-5	-15	-30	-62	-144
Subject 9	-23	-234	-300	-403	-411	-367	-266	-162
Subject 10	245	-64	-133	-311	-405	-468	-500	-830
Subject 11	1026	499	49	37	-9	-49	-88	-170
Mean	**198**	**38**	**-61**	**-124**	**-148**	**-165**	**-194**	**-242**
SEM	**323**	**236**	**183**	**217**	**208**	**178**	**205**	**308**

Supplementary Figure S1. Plot of the residuals (mean± SD) (Modeled – True /Modeled) to indicate the quality of the model fit is shown for the duration of the fit which included a meal at the beginning and a meal at the end. Notice that there is generally no bias in the residuals, except at the end, where there is a negative bias. Some of the subjects demonstrated an increase in glucose levels immediately prior to their first MRI without any meal or glucose infusion as the cause. This increase was likely due to stress and the resulting decrease in insulin sensitivity. Since our model did not capture this type of a stress-induced insulin sensitivity change, there is bias in the adjusted glucose values at this meal.

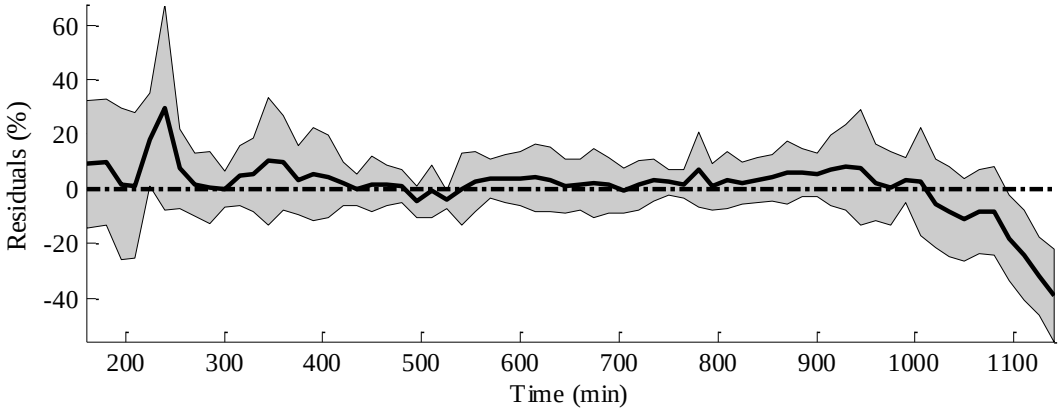

SUPPLEMENTARY DATA

^{13}C MRS Methods

The ^{13}C glucose C1 carbon in glycogen is highly deshielded, resulting in a downfield shift of ~100.5 ppm. This resonance is found in a vacant window in the ^{13}C NMR spectrum and may therefore be easily identified and quantified to allow the determination of in vivo glycogen concentrations.

Coil Design and Setup

Liver glycogen levels were determined on a 7 T Siemens MAGNETOM whole body MRI scanner. This machine is not equipped with whole body coils. It is therefore necessary for both ^{1}H and ^{13}C channels to be able to transmit and receive. In previous work Roden and co-workers described a method for correcting the liver volumes that involved sequential imaging experiments in different MRIs (4). We found that such an approach is not ideal. It is better to acquire ^{1}H images as part of a single data acquisition sequence on the same MRI scanner. To facilitate ^{1}H anatomical imaging and ^{13}C MRS within a single imaging protocol a concentric dual-tuned surface coil was constructed.

An 8 cm in diameter (1 cm wide) copper ^{13}C coil with a concentric 10 cm in diameter (1 cm wide) copper ^{1}H coil was constructed. The coils were sandwiched between 12 × 12 cm acrylic. To hold the coil assembly in place on the subject during scanning the entire assembly was placed in a home built neoprene belt with an attached pocket of sufficient size to snugly hold the coil assembly. This neoprene belt was designed to accept a small acrylic bridge to which was attached an intact ampule of 99% enriched $CH_3{}^{13}CN$ (1 mL, Sigma-Aldrich). The ampule was held 4.5 cm from the coil surface on the opposite side from the subject. The $CH_3{}^{13}CN$ served external standard to which the intensity of the C1 glycogen signal could be compared and standardized.

Pulse Sequences

^{1}H anatomical imaging was performed acquiring 10 slices in each of the coronal, axial and sagittal planes. Acquisition parameters were as follows: FOV = 280 × 280 mm^2; slice thickness = 10 mm, with skip factor of 0.3 mm; TR = 60 ms; TE = 1.6 ms; 4 transients per slice.

The T_1 of the C1 carbon of oyster glycogen was determined *in vitro* by measuring the signal intensity of the doublet as a function of TR (TR values of 150, 180, 210, 240, 300, 360, 480, 600, 1000, 1500, 2000 and 3000 ms were used). The T_1 value obtained in this manner was 238 ms, which indicates that long relaxation delays are not necessary in the ^{13}C acquisition pulse sequence. The pulse sequence for ^{13}C MRS had to be written especially for the Siemens MAGNETOM system. In our hands, attempts to employ adiabatic excitation pulses were universally deemed unsuitable; the higher pulse powers (coil voltages) required at higher fields (7 T) made the use of adiabatic pulses unattractive. The following pulse sequence was therefore employed using a simple square excitation pulse. Acquisition parameters were as follows: excitation pulse duration = 500 μs; excitation pulse bandwidth = 20,000 Hz; excitation frequency = 74.7370 MHz; acquisition pulse power = 85 V; TR equals 160 ms; number of transients = 11,000. These acquisition parameters were employed for all ^{13}C MRS data acquisitions, both *in vivo* and *in vitro*. Although ^{1}H decoupling has been previously employed to enhance signal intensity through cross polarization in previous studies (5), it was not employed in this case. This ensured that the energy deposition associated with ^{1}H decoupling would not lead to a breach of SAR limits.

In vitro Testing and Standardization

The first step was to measure the spatial distribution of B_1 relative to the ^{13}C surface coil. The method of Ginzton (6) was employed in which a small copper disc was located “infinitely” far (200 cm) from the surface of the coil and the frequency of the resonance dip measured. The change in the resonance

frequency of the coil was then measured in 0.5 cm increments from 6.5 cm to the coil surface. The square root of the change in resonance frequency between a measured distance from the coil and infinity ($\sqrt{\delta\nu}$) is proportional to B_1 and represents the detection efficiency of the coil at that distance from the coil's surface. This measurement was performed on the axis of the ^{13}C surface coil and off-axis by half a coil radius. The coil's behavior fit perfectly with the theory describing the change in B_1 as a function of distance from the coil (6). The interrogation volume of the ^{13}C coil approximates to that of the cylinder extending out about 6 cm in either direction from the coil surface (Figure S1).

These results showed that the flip angle experienced for carbon nuclei will differ depending upon the distance of the nuclei from the coil's surface. In order to develop a more thorough understanding of the effect of pulse power and distance, the ^{13}C MRS pulse sequence was tested on an 84 mm diameter sample of 30 mL of a 1.3 M solution of $^{13}CH_3OH$ in water, doped with 17 mM nickel(II) chloride (to shorten T_1). The sample was placed directly on the axis of the coil and was moved progressively further from the coil's surface in 0.5 cm increments. The applied voltage was gradually increased from 5 to 95 V in 5 V increments. The signal intensity (averaged over sixteen transients) measured at each voltage was initially sinusoidal until a flip angle of 90 had been achieved. Thereafter increases in pulse power did not nutate the signal in the manner expected of a volume coil. Indeed the signal intensity does not reach a null point. Furthermore, it was noted that as the distance of the sample from the coil surface was increased the signal intensity, for a given pulse power, decreased in line with the voltage measurements described above. The consequences of these observations for measuring liver glycogen concentrations are simple: because the liver glycogen signal being probed lies beyond 2.5 cm from the coil surface it is necessary to apply the strongest possible pulse power to increase depth penetration, regardless of the effect on flip angle over the volume of interrogation. Since a predictable, sinusoidal nutation curve could not be generated, the effectiveness of the coil was determined by the voltage induced in the coil as described above. A pulse power of 85 V, which was as comfortably close to the power handling limits of the coil as possible, was selected for all *in vivo* experimentation.

Supplementary Figure S2. The performance of the home-built ^{13}C surface coil. The change in resonance frequency as a function of the distance of a copper disc from the coils surface (left). These data show that, except close to the coil's surface, the coil interrogates a cylindrical volume extending about 6 cm from the coil surface in either direction. The linear change in C1 glycogen signal intensity, normalized to the $CH_3{}^{13}CN$ standard, is shown (right) with spectral data (inset). These data were used as the standardization curve to determine *in vivo* hepatic glycogen concentrations.

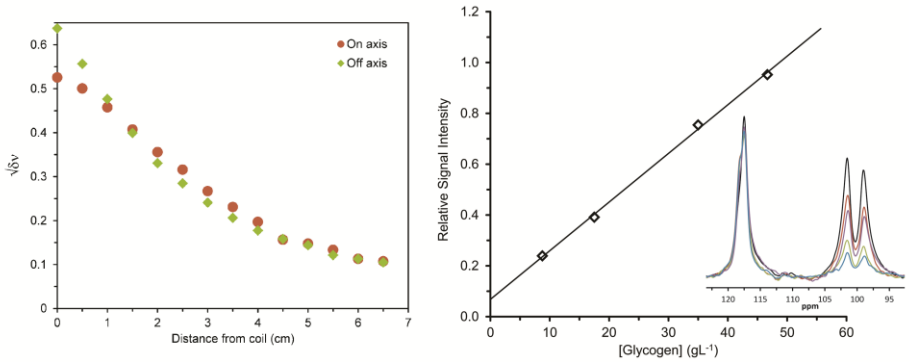

To determine that the coil was sensitive to physiologically relevant changes in glycogen concentration, the coil was tested on a phantom containing varying concentrations of oyster glycogen (7). The first step in this procedure was to determine the appropriate loading for the coil. The coil was connected to an oscilloscope, tuned and matched, and then placed on a human torso. An 18 × 18 × 5 cm container was then placed on the coil in place of the human torso. The container was filled with aqueous solutions of

sodium chloride of varying concentrations until effect of the solution on the coil loading was identical to that of the human torso. A 40 mM NaCl solution was found to load the coil equivalently to the human torso. A 14 × 14 × 9 cm container was filled with candle wax to a depth equal to 2.5 cm from the base of the container. The remaining volume was filled with solutions of oyster glycogen, in 40 mM aqueous NaCl, of varying glycogen concentration. The external standard ($CH_3{}^{13}CN$) was placed in the neoprene belt, the coil was supported by an empty 14 × 14 × 9 cm container and the wax/glycogen phantom placed on top of the coil. Spectra of the phantom were acquired, varying the glycogen concentration in the phantom, using the pulse sequence described above, which would also be used for *in vivo* data acquisition. These data (Figure S1, right) showed that the surface coil was sensitive to changes in glycogen concentration over a physiologically relevant concentration (7), and furthermore provided data to generate a standardization curve by which *in vivo* liver glycogen concentrations could be determined.

In Vivo Testing

The function of the dual-tuned surface coil was examined *in vivo* on 5 healthy subjects. The coil was placed on the right intercostal margin of each subject, the bottom of the coil was aligned with the lowest rib during inhalation, and held in place by the aforementioned neoprene belt. For these data acquisitions the $CH_3{}^{13}CN$ external standard was not in place. Subjects were positioned within the magnet such that the center of the surface coil was at iso-center along the axis of the magnet. Subjects were placed as far to the left of the magnet as practicable so as to position the liver as close iso-center as possible. Scout ^{1}H imaging was performed to ensure that the coil location did in fact cover liver volume on the subject. The known movement of liver within the torso was a constant concern and vertical realignment of the coil was occasionally necessary. Once the coil had been satisfactorily located during baseline data acquisition, its position was marked on the subject's torso and located in an identical position for all subsequent data acquisition sessions. ^{1}H anatomical imaging studies were performed first. With anatomical data in hand, the ^{13}C MRS data were then acquired.

In Vivo Data Acquisition

^{1}H anatomical images and ^{13}C MRS data were acquired on 11 subjects with type 1 diabetes using an identical data acquisition protocol to that described for *in vivo* testing on healthy subjects without diabetes. For subjects with diabetes, data were acquired on 4 occasions; an initial study after 8 hours of feeding on a control diet; after 13 hours of fasting; and then again after 8 hours of feeding a controlled diet; and after 13 hours of fasting. The first two baseline data acquisitions were performed prior to administration of glucagon, the latter 2 after scheduled administrations of glucagon at a dose of 2 $mgkg^{-1}$, for a total of 8 doses. Of the 11 subjects recruited into the study data from three subjects had to be excluded from analysis. Data were not obtained for the first subject due to an error in equipment set-up. Insufficient signal-to-noise for hepatic glycogen was obtained in all four scans for another subject due to excessive separation of the coil from the liver by a subcutaneous adipose layer. A third subject was unable to complete the four MRS data acquisitions.

Data Analysis

The ^{13}C FID of each MR exam was treated using the NUTS NMR software (ACORNsoft) (8). Line broadening of 30 Hz was applied to each FID, followed by an exponential multiplication prior to Fourier transformation. After phasing, the baseline of each spectrum was flattened using the 'baseline fit' routine in the NUTS program. The signal intensities of the $CH_3{}^{13}CN$ and C1 glycogen peaks were then determined using the peak fitting routine of the NUTS program, allowing the routine to determine the appropriate Lorenzian/Guassian weighting of each peak. The ratio of C1 glycogen to $CH_3{}^{13}CN$ was then calculated for each exam. To determine the concentration of glycogen in the liver from this number it

was first necessary to account for the difference in liver and glycogen standard volume within the cylinder interrogation of the coil.

To accomplish this two ^{1}H images: one axial, one sagittal, were selected. The images selected were from as close to the middle of the coil as possible, based upon the location of hyper-intense regions located on the dermis that revealed the position of the ^{1}H coil. By measuring the distance between them and comparing with the known diameter of the ^{1}H surface coil it was possible to select an image from the middle of the coil. Each image was then carefully treated in the following manner: a grid was the placed over the image, the grid was scaled such that its total size represented 9 cm × 6 cm of the established region interrogated by the coil. The grid comprised cells of 0.5 × 0.5 cm cells extending a distance of 2.5 cm to 6 cm from the coil surface. No liver was found to lie within 2.5 cm of the coil surface. The grid was rotated in such a way as to reflect the coil lying flat across the intercostal margin of the subject. In the case of sagittal images, Pythagoras's theorem was employed to account for the oblique angle of the coil relative to the plane of data acquisition. The application of these grids is shown schematically (Figure S2, left). The area of each grid cell occupied by liver was then calculated by using the "Sketch and Calc" online application (9). The area occupied by liver in each row of the grid in each image was summed and the axial and sagittal areas multiplied.

Supplementary Figure S3. Volume correction in analyzing the ^{13}C MRS data for the glycogen C1 signal. Left: a schematic representation of the grid system used to account for the location of the liver. a) a representation of the position of the grids relative to the surface coil and the axial (blue), coronal (red) and sagittal (green) acquisition planes. b) a representative axial ^{1}H image. c) a representative sagittal ^{1}H image. Right and Center: the effect of correcting MRS data for liver volume changes, the black data are the average of 8 subjects the blue and red data are data for individual subjects with outlying data points.

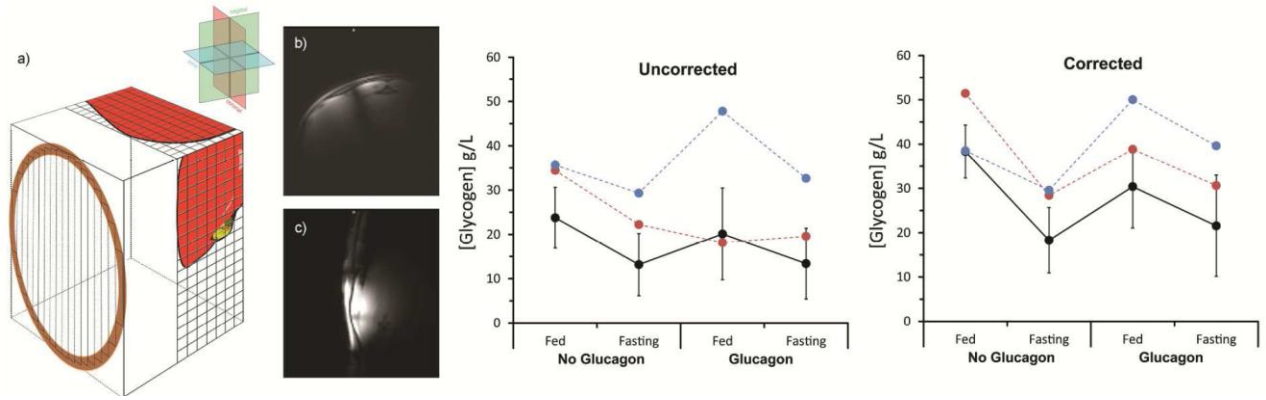

This afforded the liver volume at each 0.5 cm incremental from the coil surface. However, to obtain the relative signal intensity arising from this liver volume it is necessary to account for the variation in flip angle that occurs as a distance from the coil increases. This is achieved by multiplying the liver volume at each 0.5 cm increment from the coil surface by a proportionality constant, accounting for the flip angle, derived from the coil sensitivity tests (*vide supra*). It should be noted that the absolute flip angle at each distance from the coil need not be known. The same proportionality constant was applied to the oyster glycogen phantom (each grid unit in this case is completely occupied). By dividing the sum of the product of proportionality constant and the liver volume in each row for the in vivo data by the same sum for the glycogen phantom it is possible to obtain a "fill factor" for each data acquisition session. Multiplying the experimentally obtained *in vivo* glycogen C1 signal intensity by the fill factor allows us to directly correlate the *in vivo* signal intensity with the standardization curve is derived from the

glycogen phantom without the need to know the exact value of the flip angle at each distance from the coil. This allowed the relative intensity of the ^{13}C signal to be compared to that obtained from the standardization curve and the concentration of glycogen in the liver to be determined in gL^{-1}.

The importance of such a volume correction method is made clear by the data presented (Figure S2, right and center) which show the overall results of all 8 subjects with diabetes included in the study both with and without volume correction. When no volume correction is applied to the data the overall level of liver glycogen in all cases are typically found to be somewhat low – usually less than 40 gL^{-1} even when well fed. One subject was found to have improbably low liver glycogen concentrations – below 15 gL^{-1} in all studies. However, analysis of the ^{1}H images showed that in this case the liver was separated from the coil surface by a larger distance than in all other subjects and thus a comparatively small liver volume was being interrogated. Once the volume correction was applied the liver glycogen levels were found to lie closer to the average across all subjects studied. The data for six of the test subjects with diabetes showed a clear, consistent and expected trend. In contrast, the data for the other two test subjects with diabetes contained one or more data points that lay outside this trend. These data are shown individually in Figure S2, right and center. In one case the uncorrected data shows the subject has about 13% less liver glycogen (<20 gL^{-1}) when fed with glucagon than when fasting either with or without glucagon (Figure S2, red data). Analysis of the axial and sagittal ^{1}H images revealed that in both of these cases the liver had moved substantially from scan to scan and the liver occupied significantly different fraction of the volume interrogated by the coil in one or more scans and this gave rise to "out-of-trend" data. After the volume correction had been properly applied these data follow the same trend as those for all the other subjects. The uncorrected data shows that second subject has substantially (34%) more liver glycogen (~50 gL^{-1}) when fed with glucagon than fed without glucagon (Figure S2, blue data). Although applying the volume correction to this dataset is found to reduce the difference slightly (to 29%) it does not bring the dataset into complete alignment with the other subjects. The benefit of applying volume correction in this case is that it shows that this datum is not anomalous. It is important to note that when volume correction is applied to these data the liver glycogen concentrations determined for all subjects are much closer to the accepted concentrations of liver glycogen expected in well fed humans (7). This demonstrates the critical importance of proper analysis of volume fraction correction when assessing liver glycogen concentrations in this manner. No account was taken of any contribution to the glycogen signal arising from subcutaneous muscle, consistent with previously reported observations (10).

SUPPLEMENTARY DATA

References

1. Wilinska ME, Chassin LJ, Schaller HC, Schaupp L, Pieber TR, Hovorka R. Insulin kinetics in type-I diabetes: Continuous and bolus delivery of rapid acting insulin. IEEE Trans Biomed Eng 2005;52:3-12

2. Hovorka R, Canonico V, Chassin LJ, Haueter U, Massi-Benedetti M, Orsini Federici M, Pieber TR, Schaller HC, Schaupp L, Vering T, Wilinska ME. Nonlinear model predictive control of glucose concentration in subjects with type 1 diabetes. Physiol Meas 2004;25:905-920

3. Wolever TM. Effect of blood sampling schedule and method of calculating the area under the curve on validity and precision of glycaemic index values. Br J Nutr 2004;91:295-301

4. Bischof MG, Krssak M, Krebs M, Bernroider E, Stingl H, Waldhausl W, Roden M. Effects of short-term improvement of insulin treatment and glycemia on hepatic glycogen metabolism in type 1 diabetes. Diabetes 2001;50:392-398
5. Jue T, Rothman DL, Tavitian BA, Shulman RG. Natural-abundance 13C NMR study of glycogen repletion in human liver and muscle. Proc Natl Acad Sci U S A 1989;86:1439-1442

6. Ginzton EL. *Microwave measurements. Microwave measurements.* New York, McGraw-Hill, 1957

7. Carroll NV, Longley RW, Roe JH. The determination of glycogen in liver and muscle by use of anthrone reagent. J Biol Chem 1956;220:583-593

8. Acorn NMR Inc. NMR Utility Transform Software (NUTS) [computer program]. Version 6.1. Livermore, CA: 2011.

9. Dobbs E. SketchAndCalc. Area Calculator. http://www.sketchandcalc.com [computer program]. Version 4.1.3. 2013.

10. Tomiyasu M, Obata T, Nonaka H, Nishi Y, Nakamoto H, Takayama Y, Ikehira H, Kanno I. Evaluating glycogen signal contamination in muscle by (13)C MRS of the liver. Magn Reson Imaging 2008;26:572-576